Approximation constant-Q reverse time migration in the time domain: Unsplit-field PML formulation

Ali Fathalian and Kris Innanen

ABSTRACT

We investigate the simulation of wave propagation in attenuation medium within approximating constant-Q. Such wave propagation can be modelled with a finite difference scheme by introducing a series of standard linear solid (SLS) mechanisms, and it can be carried out within a computationally tractable region by making use of perfectly-matched layer (PML) boundary conditions. To consider the effects of the number of relaxation mechanisms (L), we compare numerical and analytical solution of the wave equation for a homogeneous and complex medium. In the weak attenuation ($Q = 100$), the numerical solutions using a series of SLS relaxation mechanisms and analytical solutions agree very well, and the acoustic and viscoacoustic RTM images have similar artifacts and amplitudes in the shallow layers. At the deeper layers, we can see that a series of SLS mechanisms RTM yield comparable results with the acoustic RTM case. In strong attenuation ($Q = 20$), when the wave reaches greater depth, the error of numerical solutions using single SLS mechanism increase and the viscoacoustic RTM images using a single SLS mechanisms are not so accurate in the deeper layers. Although the results of single SLS relaxation mechanism are still useful for practical application, the three SLS relaxation mechanisms are quite accurate for both weak and strong attenuation.

INTRODUCTION

Attenuation is an increasingly indispensable component of wavefield simulation in seismic exploration and monitoring applications. It is a key element in many recent instances of data modelling, reverse time migration (RTM), and full waveform inversion (FWI). A standard linear solid model (SLS) for attenuation is one of many mathematical Q models that describes the wave propagation. McDonal et al. (1958) perform the constant-Q model, i.e., the attenuation coefficient is considered to be approximately linear with frequency. Kjartansson (1979) use a linear model for attenuation of the wave with Q independent of frequency, which is mathematically simple and completely specified by phase velocity and Q. Liu et al. (1976) and Carcione et al. (1988) developed an efficient method based on the general standard linear solid (SLS) to simulate nearly constant Q model.
The main point in the nearly constant-Q method is the selection of the appropriate number of mechanisms, i.e., L. Although the results of single SLS relaxation mechanism are acceptable for practical application (Blanch et al., 1995), the three SLS (L=3) is considered to be accurate for weak and strong attenuations mediums(Emmerich and Korn, 1987; Savage et al., 2010). In this paper, we investigate the simulation of wave propagation in attenuation medium within approximating constant-Q using an unsplit-field viscoacoustic wave equation in the time domain. To consider the accuracy of the number of relaxation mechanisms (L), we compare numerical and analytical solution of the wave equation for a homogeneous and complex medium over a frequency band. Also, we investigate the accuracy of single, three, and five SLS relaxation mechanisms on RTM images.
This article is organized as follows. In the first section we describe the background of

research, and then the attenuation model is presented in the second section. In the third section, we introduce the unsplit-field PML formulation of the approximate constant-Q viscoacoustic wave equation. Numerical results on synthetic data are presented in the fourth section.

ATTENUATION MODEL

The 2D viscoacoustic wave field can be solved for through a system of first-order differential equations in terms of stresses and the particle velocities. In linear viscoelasticity, the basic hypothesis is that the value of the stress tensor depends upon the time-history of the strain tensor. The viscoelastic hypothesis can be expressed as (Christense, 1982)

$$\sigma = G(t) * \dot{\varepsilon}, \tag{1}$$

where $G(t)$ is the relaxation function and the symbol * denotes time convolution. The equations describing wave propagation in viscoacoustic media can be derived in terms of the stress relaxation function. The constant-Q model for attenuation is linear with frequency and obtain by applying properties of the convolution and then transforming Equation 1 to the frequency domain as

$$\sigma(\omega) = M(\omega)\varepsilon(\omega), \tag{2}$$

where $M(\omega)$ is the complex relaxation modulus, and ω is the angular frequency. The attenuation effects described by the quality factor and the phase velocity dispersion. The quality factor is given by Carcione et al. (1988)

$$Q(\omega) = Re[M(\omega)]/Im(M(\omega)), \tag{3}$$

where Re and Im are the real and imaginary parts, respectively. The frequency-dependent phase velocity is the angular frequency divided by the real wavenumber

$$\upsilon_p(\omega) = (Re[\sqrt{\rho/M(\omega)}])^{-1}, \tag{4}$$

where ρ is the medium density.
To investigate the attenuation effects model of absorption mechanism must be defined. We consider the generalized standard linear solid model (GSLS) to obtain a nearly constant quality factor (Liu et al., 1976) over the frequency range. The complex modulus of a GSLS can express in the frequency-domain as

$$M(\omega) = M_R \left[1 - L + \sum_{l=1}^{L} \frac{1 + \omega\tau_{\varepsilon l}}{1 + \omega\tau_{\sigma l}}\right], \tag{5}$$

where M_R is the relaxed modulus, and $\tau_{\sigma l}$ and $\tau_{\varepsilon l}$ are the stress and strain relaxation times given by

$$\tau_{\sigma l} = \frac{\sqrt{1 + 1/Q_{0l}^2} - 1/Q_{0l}}{\omega}, \tag{6}$$

$$\tau_{\varepsilon} = \frac{1}{\omega^2 \tau_{\sigma l}}.$$

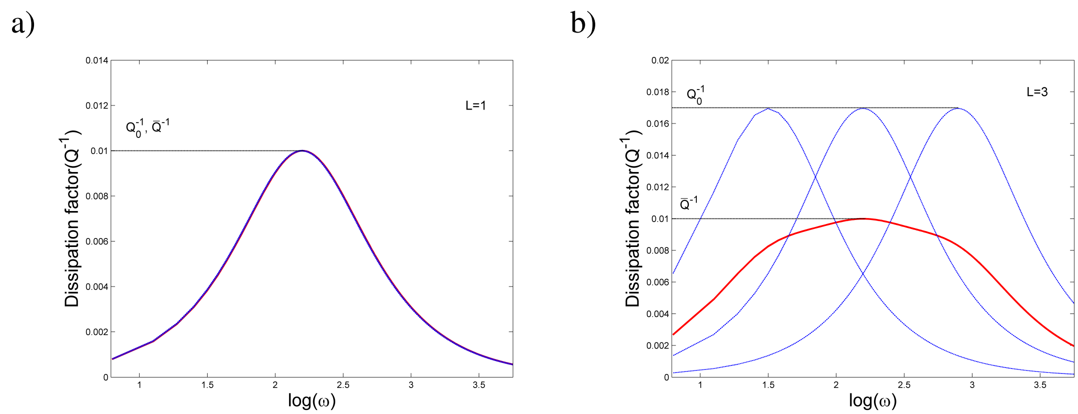

FIG. 1. The dissipation factor of single standard linear solid (a) and three SLS mechanisms (b). In this case $\bar{Q} = 100$, the system is composed of L relaxation peaks of maximum value of Q_0^{-1} each, and equally distributed in the $log(\omega)$ scale.

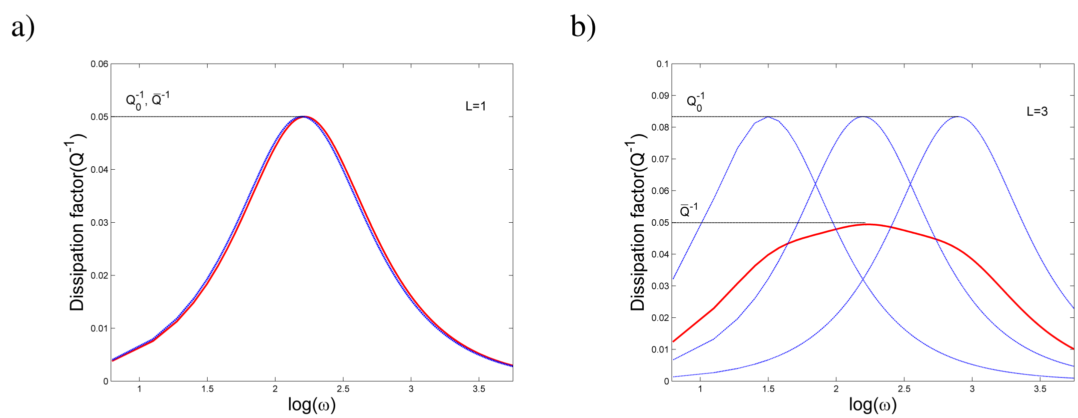

FIG. 2. The dissipation factor of single standard linear solid (a) and three SLS mechanisms (b). In this case $\bar{Q} = 20$, the system is composed of L relaxation peaks of maximum value of Q_0^{-1} each, and equally distributed in the $log(\omega)$ scale

Where ω and Q_{0l} are the center angular frequency of relaxation peak, and the minimum quality factors respectively. The experiment results have shown that the earth materials have constant Q over a limited range of frequency (Bourbie et al., 1987). Therefore the quality factor is usually considered to be constant in the exploration frequency bandwidth. For generalized standard linear solid model (GSlS), the quality factor is

$$Q = \frac{Re[M(\omega)]}{Im[M(\omega)]} = \frac{1 + \sum_{l=1}^{L} \frac{\omega^2 \tau_{\sigma l}^2}{1+\omega^2 \tau_{\sigma l}^2} \tau}{\sum_{l=1}^{L} \frac{\omega \tau_{\sigma l}}{1+\omega^2 \tau_{\sigma l}^2} \tau}, \tag{7}$$

where $\tau = (\tau_{\varepsilon l}/\tau_{\sigma l}) - 1$ (Blanch 1995). By applying the approximation $\tau_{\varepsilon l} \approx \tau_{\sigma l}$ the dissipation factor (Q^{-1}) for single mechanism can be obtained as (Bourbie et al., 1987):

$$Q^{-1} = \frac{\omega(\tau_\varepsilon - \tau_\sigma)}{1 + \omega^2 \tau_\sigma \tau_\varepsilon}, \tag{8}$$

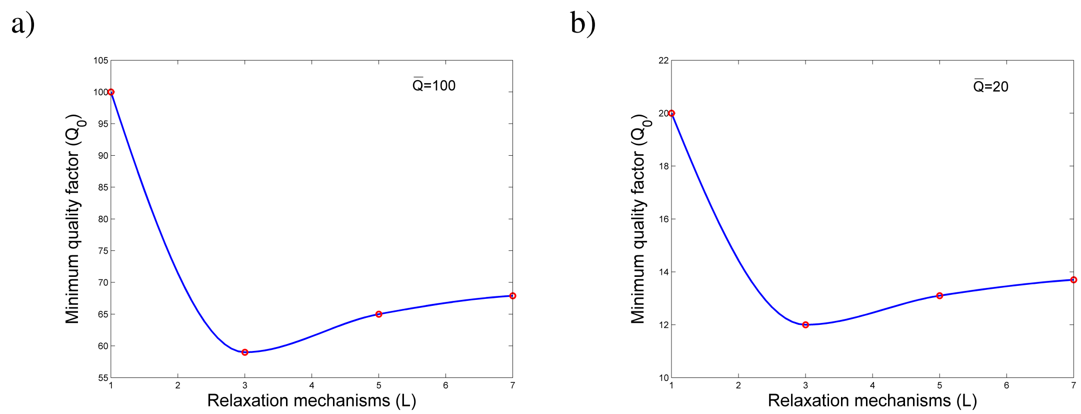

FIG. 3. The effect of increasing number of mechanisms on minimum quality factor for (a) constant $\bar{Q} = 100$, and (b) constant $\bar{Q} = 20$.

With Eqs. (1) and (4) and assumption $\tau_{0l} = (\tau_{\sigma l}\tau_{\varepsilon l})^{1/2}$ and $Q_{0l} = 2\tau_{0l}/\tau_{\varepsilon l} - \tau_{\sigma l}$ (Casula and Carcione, 1992)the seismic quality factor Q for a GSLS can be obtained as:

$$Q = Q_0 L \left(\sum_{l=1}^{L} \frac{2\omega\tau_{0l}}{1 + \omega^2\tau_{0l}^2} \right)^{-1}, \tag{9}$$

The almost constant quality factor is a quality factor at central of frequency band, $Q(\omega_0) = \bar{Q}$, thus

$$\bar{Q} = Q_0 L \left(\sum_{l=1}^{L} \frac{2\omega_0\tau_{0l}}{1 + \omega_0^2\tau_{0l}^2} \right)^{-1}. \tag{10}$$

Using Equation 10, we consider the dissipation factor for different value of constant Q over a broad frequency range(between $5Hz$ and $125Hz$). The dissipation factor of single and three pairs of relaxation mechanisms for constant Q of 100 displayed in Figure 1. The dissipation factor of constant Q is a match to the dissipation factor of minimum quality factor $Q0$ and represents a single relaxation peak at $\omega_0 = 1/\tau_0$ (Figure 1a). In Figure 1b we study the dependence of dissipation factor on the number of single standard linear elements. For L=3, the curve composed of 3 single mechanisms each with maximum dissipation factor $Q0^{-1}$. However, to consider the series of a single standard linear solid model with the accurate approximation of constant $\bar{Q}$ the minimum quality factor $Q0$ must be calculated correctly. Similarly, in Figure 2 the dissipation factor for single and three pairs of relaxation mechanisms for constant quality factor $\bar{Q} = 20$ are displayed. The effect of increasing number of mechanisms on minimum quality factor shown in Figure 3.
In order to investigate the accuracy of a series of single standard linear solid mechanisms, the dissipation factor (Q^{-1}) and phase of the velocity of five, three, and one SLS mechanisms compared with the theoretical model. The reference phase velocity is $2.5km/s$, and the reference band is $5 - 125Hz$. For $Q = 100$, the three SLS fits the theoretical model curves very well in the central frequency. Note, the one, and five SLS have a good approximation to the phase velocity and dissipation factor around the reference frequency (Figure 4). In Figure 5 the dissipation factor and phase velocity of five, three and one SLS mechanisms for the strong attenuation case are compared with the theoretical model. In

this case, We found the three SLS mechanisms fit the theoretical model curves in the central frequency, and the single and five SLS mechanisms have a good approximation to the phase velocity and dissipation factor around the center frequency.

UN-SPLIT PML FORMULATION FOR VISCOACOUSTIC WAVE

The wave equation of the GSLS model based viscoacoustic medium theory expressed as follows (Robertsson et al., 1994):

$$\begin{aligned} \frac{\partial u_x}{\partial t} &= -\frac{1}{\rho}\frac{\partial P}{\partial x}, \\ \frac{\partial u_z}{\partial t} &= -\frac{1}{\rho}\frac{\partial P}{\partial z}, \end{aligned} \tag{11}$$

$$\frac{\partial P}{\partial t} = -M_R\left(\frac{\partial u_x}{\partial x}+\frac{\partial u_z}{\partial z}\right)\left[1-\sum_{\ell=1}^{L}\left(1-\frac{\tau_{\varepsilon\ell}}{\tau_{\sigma\ell}}\right)\right]-\sum_{\ell=1}^{L} r_\ell, \tag{12}$$

$$\frac{\partial r_\ell}{\partial t} = -\frac{1}{\tau_{\sigma\ell}}r_\ell+\rho c_p^2\left(\frac{\partial u_x}{\partial x}+\frac{\partial u_z}{\partial z}\right)\frac{1}{\tau_{\sigma\ell}}\left(1-\frac{\tau_{\varepsilon\ell}}{\tau_{\sigma\ell}}\right), 1\leq \ell \leq L, \tag{13}$$

where $u_x(x,t)$ and $u_z(x,t)$ are the particle velocity components in the x- and z-directions respectively. $P(x,t)$ is pressure wavefield , $\rho(x)$ is density, and r_ℓ are referred to as memory variables (Carcione et al., 1988). In order to introduce the PML boundary for such viscoacoustic waves, the first-order linear differential equations are modified using the complex coordinate stretching approach. In the frequency domain, derivative operators replaced as follows

$$\begin{aligned} \partial_x &\rightarrow \left[1+\frac{id(x)}{\omega}\right]\partial_x, \\ \partial_z &\rightarrow \left[1+\frac{id(z)}{\omega}\right]\partial_z. \end{aligned} \tag{14}$$

By applying the complex coordinate stretching to the first-order linear differential Equations 11, 12, and 13 in the frequency domain and transforming back to the time domain (Fathalian and Innanen, 2016) the unsplit-field PML equations of the GSLS model based viscoacoustic medium theory can obtain as

$$\begin{aligned} \frac{\partial P}{\partial t} &= -K\left[\frac{\partial(u_x+d(z)u_x^{(1)})}{\partial x}+\frac{\partial(u_z+d(x)u_z^{(1)})}{\partial z}\right]\left[1-\sum_{\ell=1}^{L}\left(1-\frac{\tau_{\varepsilon\ell}}{\tau_{\sigma\ell}}\right)\right] \\ &\quad -\left[d(x)+d(z)\right]P-d(x)d(z)p^{(1)}-\sum_{\ell=1}^{L} r_\ell, \end{aligned} \tag{15}$$

a)

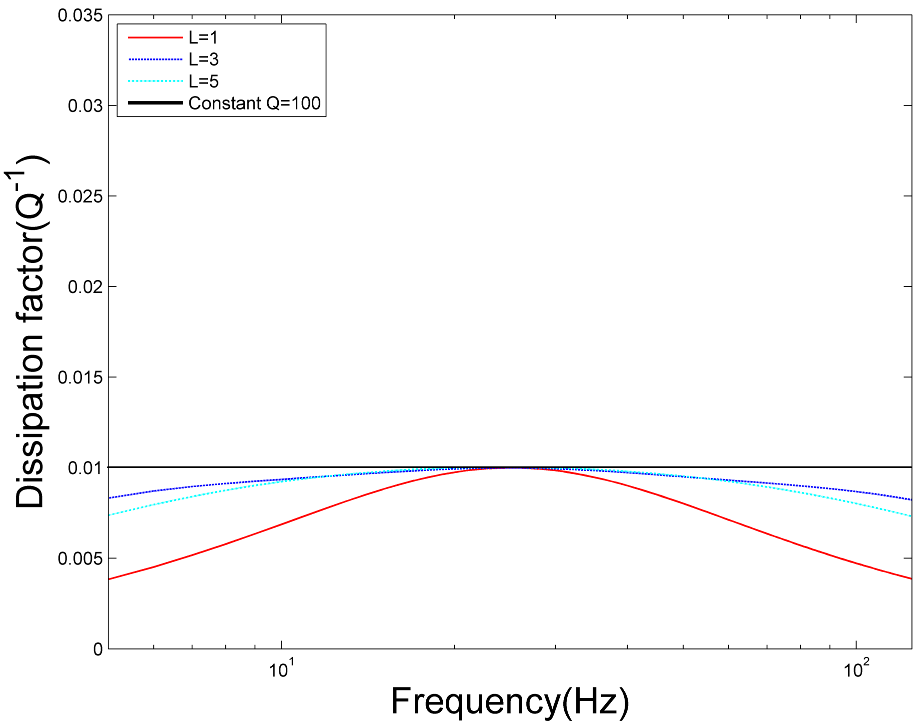

b)

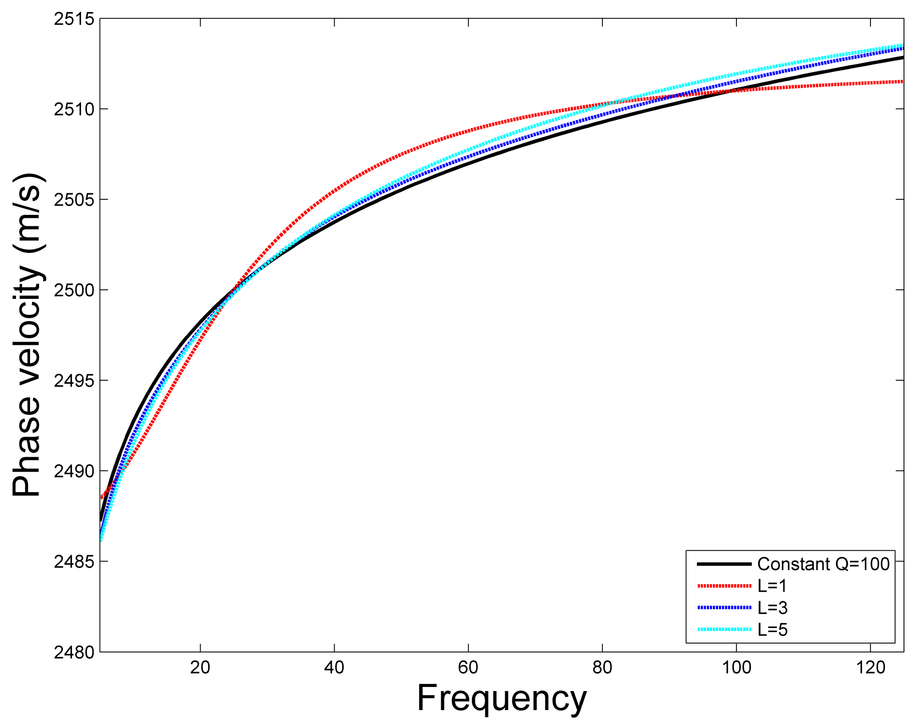

FIG. 4. The dissipation factor (a) and phase velocity (b) of constant $Q = 100$. The black line corresponds to constant $Q = 100$, red line corresponds to one SLS ($Q_0 = 100$), blue line corresponds to three SLS ($Q_0 = 59$), and cyan line corresponds to five SLS ($Q_0 = 65$).

a)

b)

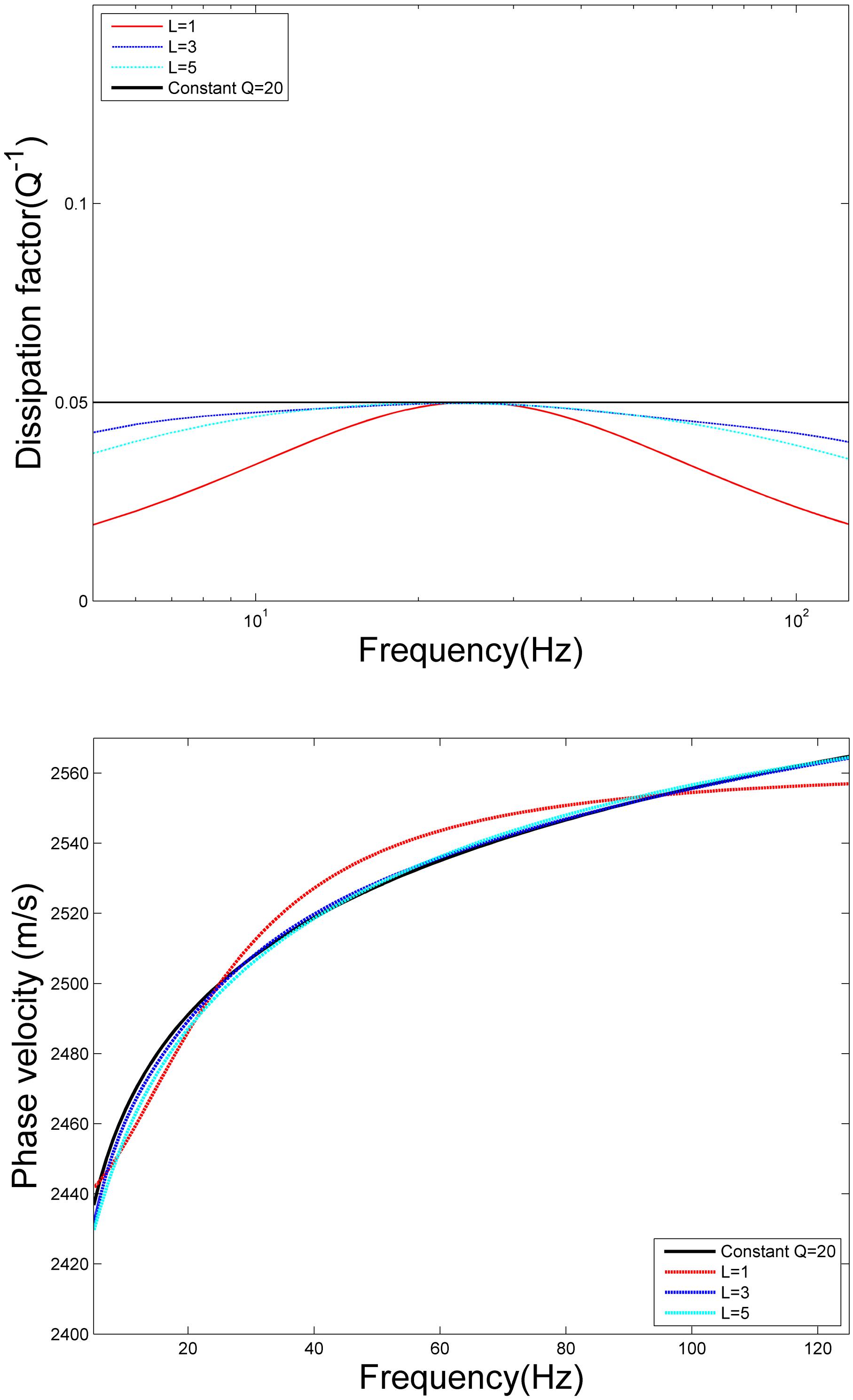

FIG. 5. The dissipation factor (a) and phase velocity (b) of constant $Q = 20$. The black line corresponds to constant $Q = 20$, red line corresponds to one SLS ($Q_0 = 20$), blue line corresponds to three SLS ($Q_0 = 11.9$), and cyan line corresponds to five SLS ($Q_0 = 13.1$).

$$\frac{\partial u_x}{\partial t} = -\frac{1}{\rho}\frac{\partial P}{\partial x} - d(x)u_x, \tag{16}$$

$$\frac{\partial u_z}{\partial t} = -\frac{1}{\rho}\frac{\partial P}{\partial z} - d(z)u_z, \tag{17}$$

$$\begin{aligned}\frac{\partial r_l}{\partial t} &= -\frac{1}{\tau_\sigma}r_l + K\left[\frac{\partial(u_x + d(z)u_x^{(1)})}{\partial x} + \frac{\partial(u_z + d(x)u_z^{(1)})}{\partial z}\right]\frac{1}{\tau_{\sigma l}}\left(1 - \frac{\tau_{\varepsilon l}}{\tau_{\sigma l}}\right) \\ &\quad - [d(x) + d(z)]\, r_l - d(x)d(z)r_l^{(1)}.\end{aligned} \tag{18}$$

where the auxiliary variables $u_x^{(1)}$, $u_z^{(1)}$, $P^{(1)}$, and $r^{(1)}$ are the time-integrated components for velocity, pressure, and memory variable fields. They defined as

$$\begin{aligned} u_x^{(1)}(X,t) &= \int_{-\infty}^{t} u_x(X,t^{'})dt^{'}, \\ u_z^{(1)}(X,t) &= \int_{-\infty}^{t} u_z(X,t^{'})dt^{'}, \\ P^{(1)}(X,t) &= \int_{-\infty}^{t} P(X,t^{'})dt^{'}, \\ r^{(1)}(X,t) &= \int_{-\infty}^{t} r(X,t^{'})dt^{'}. \end{aligned} \tag{19}$$

To consider the effects of the number of relaxation mechanisms (L), we compare numerical and analytical solution of the wave equation for a homogeneous medium with a background velocity of 2500 m/s for different values of quality factor ($Q = 20$, and $Q = 100$). In Figure 6a depth profiles of the wavefield extracted at three different times with $Q = 100$ are plotted. In the weak attenuation case($Q = 100$), As the wave begins to propagate, the numerical and analytical solutions agree very well. And when the propagation time increases and the wave reached greater depth, the single SLS mechanism is still significant compared to the analytical results. For strong attenuation ($Q = 20$), the numerical results (FD) and analytical solution displayed in Figure 6b. The numerical and analytical solution match very well but wave the reaches greater depth, the single SLS mechanism not matched with the analytical results and mismatch increases with depth.

NUMERICAL RESULTS

To investigate the accuracy of the SLS mechanisms we consider the homogenous and the Marmousi model. We examine the numerical character of the solutions of the constant-Q wave equation as created using the unsplit-field PML boundary approach. We first consider the propagation of waves in a homogeneous model. The viscoacoustic medium considered here characterized by the constant velocity model, where the size of the grid is 1001×1001. The source located at the point (2000m, 2000m) and the source signature is

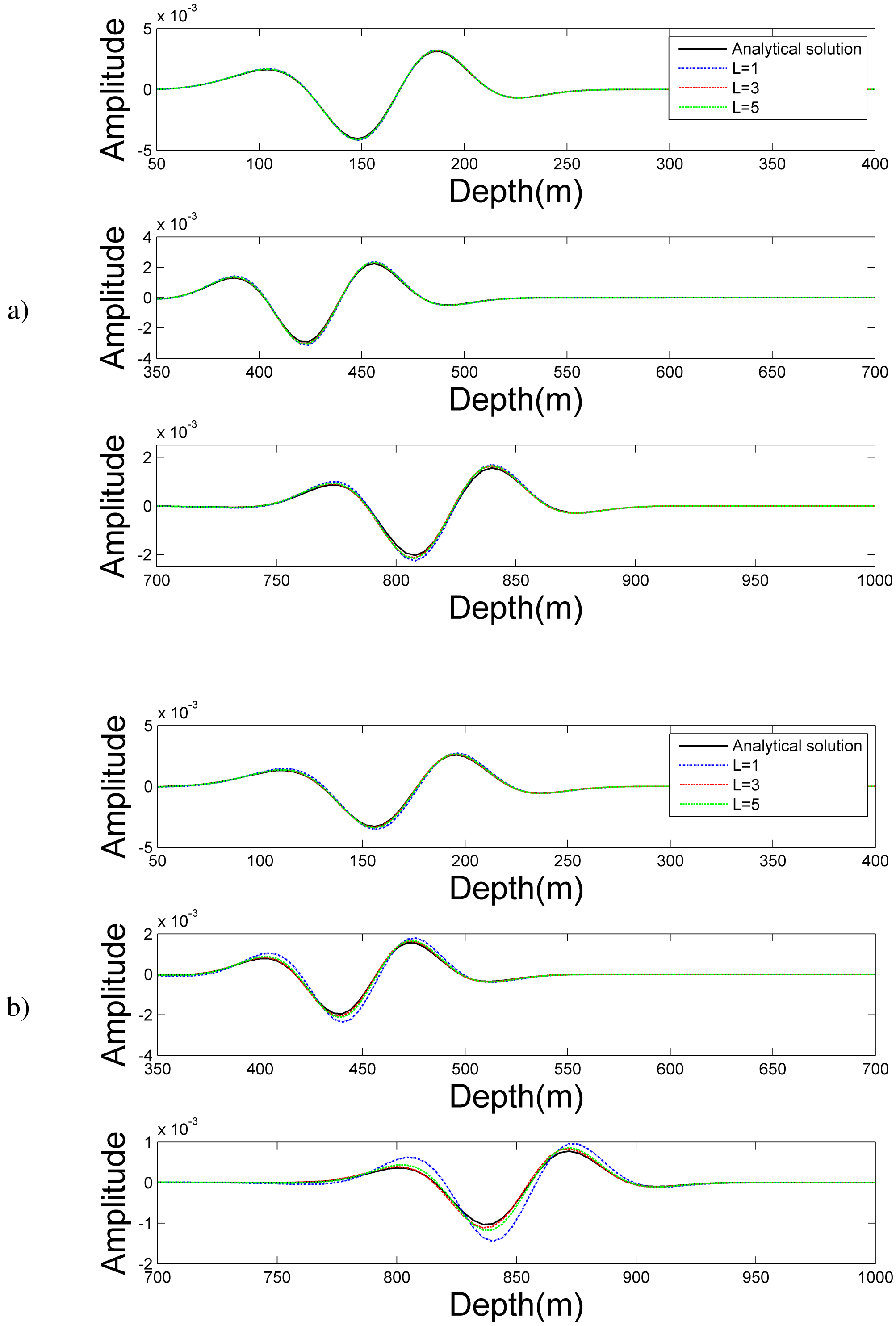

FIG. 6. Depth traces of FD and analytical solution shown at three different time steps for (a)$Q = 100$, and (b) $Q = 20$. The solid black lines, dashed blue lines, dashed red lines, and dashed green lines represent the analytical solutions, numerical solutions with L=1, L=3, and L=5 respectively.

a)

b)

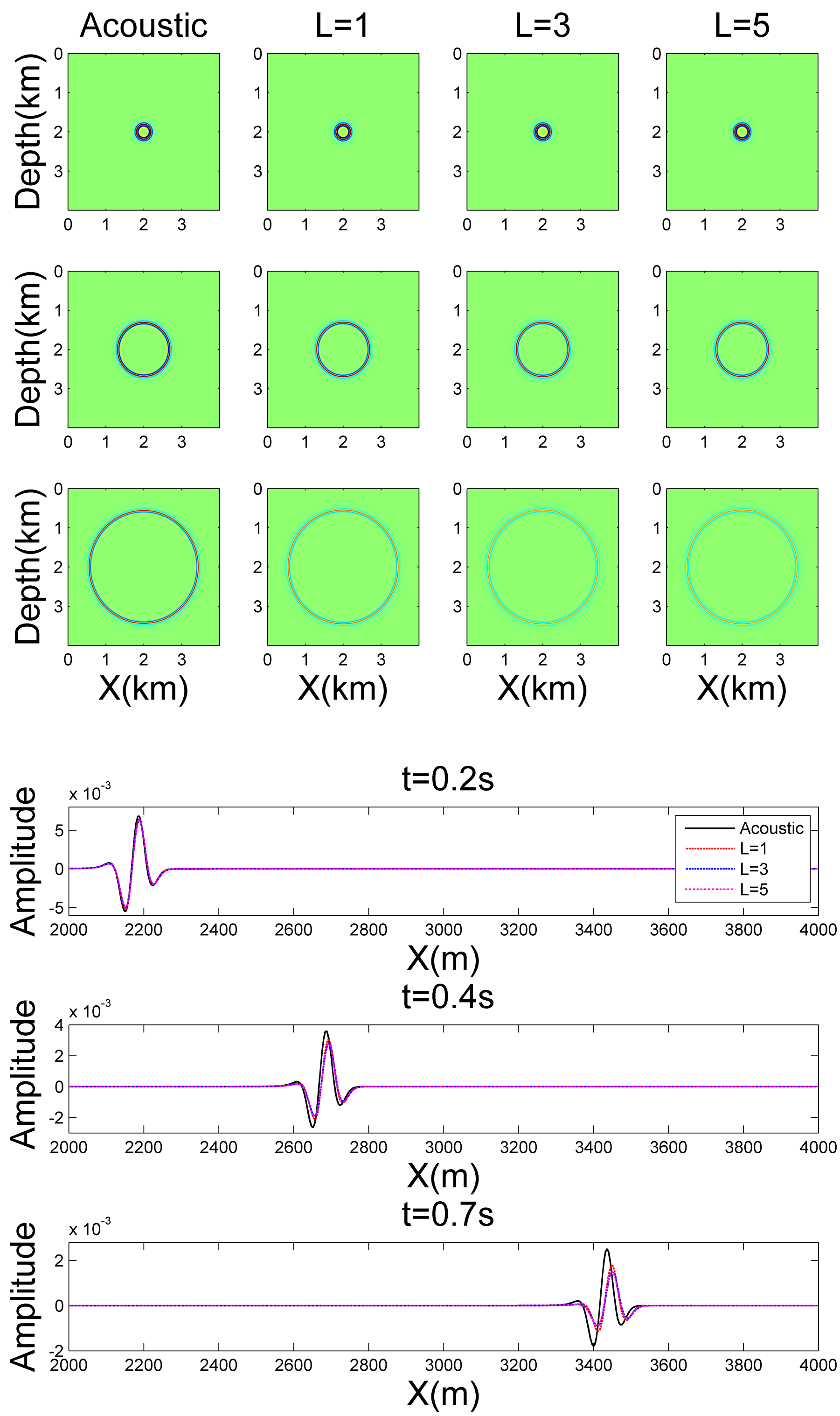

FIG. 7. (a)Snapshots showing an expanding wavefront at different time step for a acoustic medium (left panels), and for a medium with attenuation ($Q = 100$) with three mechanisms ($L = 1$, $L = 3$, and $L = 5$). (b) Depth traces from Figure (a) showing the effect of attenuation on the amplitude and phase of propagating wave with three different SLS.

a)

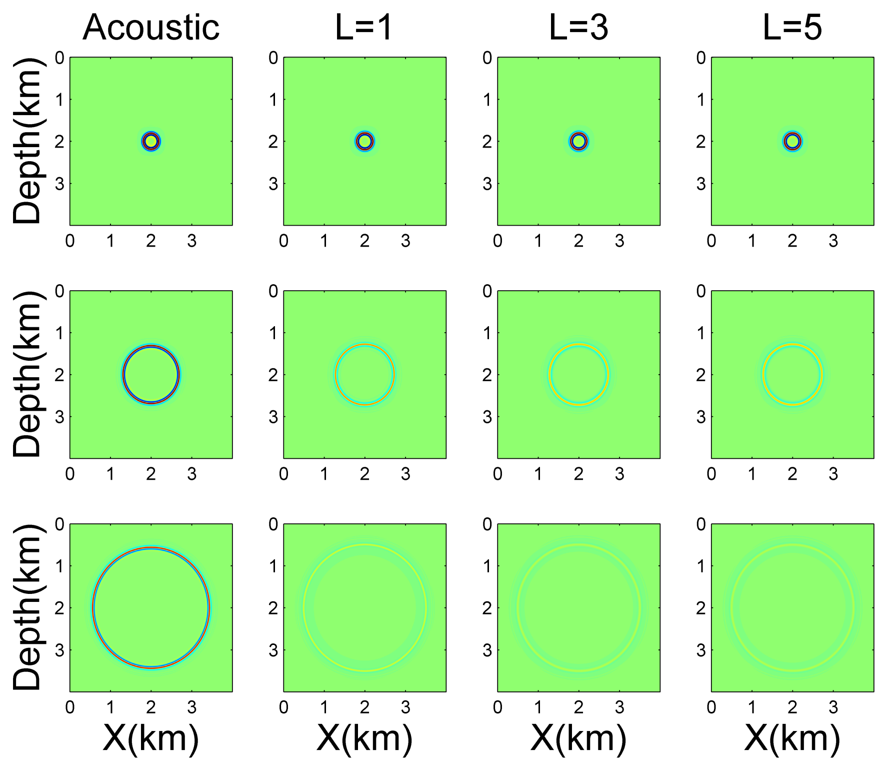

b)

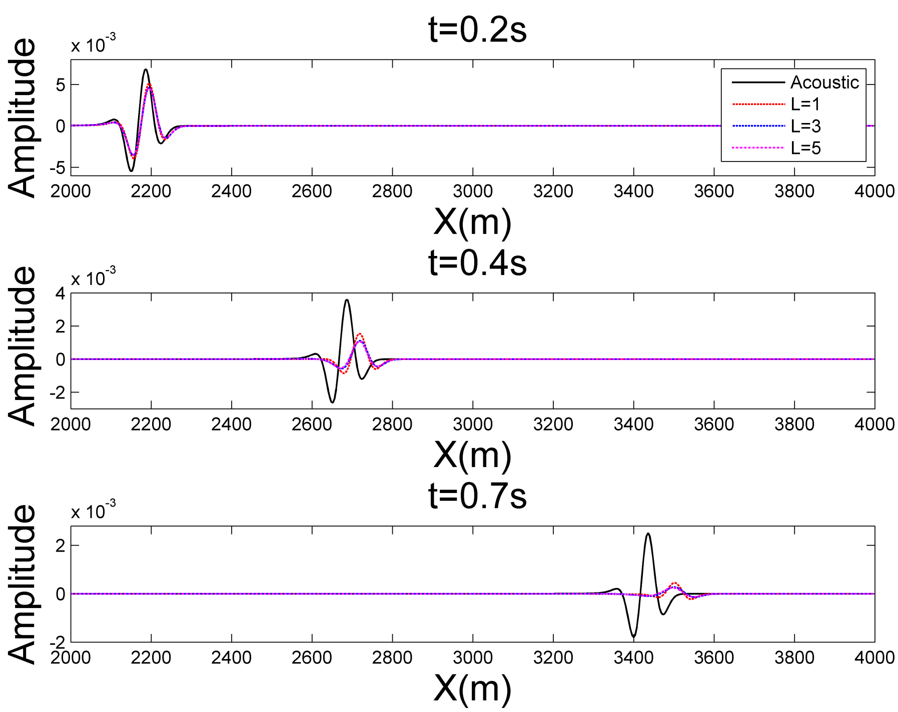

FIG. 8. (a)Snapshots showing an expanding wavefront at different time step for a acoustic medium (left panels), and for a medium with attenuation ($Q = 20$) with three mechanisms ($L = 1$, $L = 3$, and $L = 5$). (b) Depth traces from Figure (a) showing the effect of attenuation on the amplitude and phase of propagating wave with three different SLS

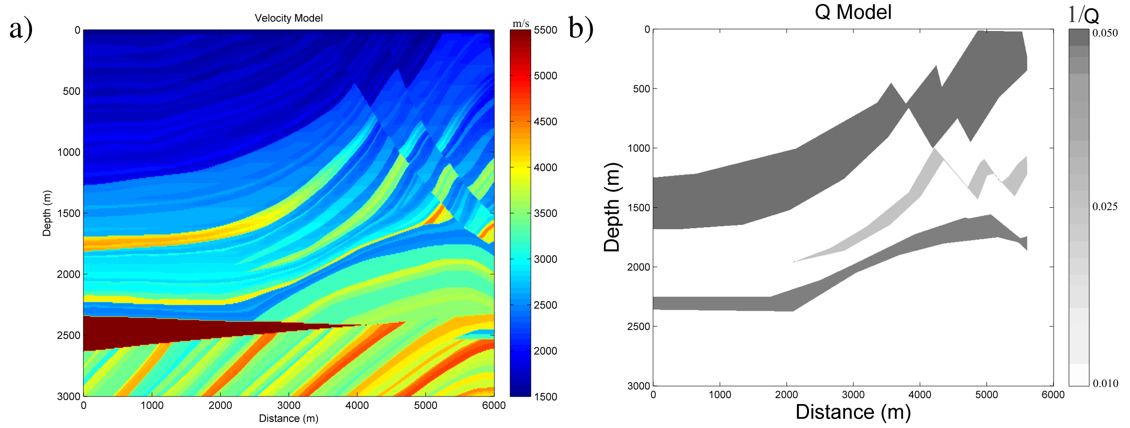

FIG. 9. Portion of the Marmousi velocity model (a) and Q model (b)..

a zero-phase Ricker wavelet with a central frequency of 25 Hz. The grid spacing in the x and z directions is 4m. An unsplit-field PML absorbing boundary condition is applied to the sides and bottom of the model. In Figure 7a snapshots of the 2D viscoacoustic wavefield with different mechanisms using the unsplit-field PML absorbing layers are plotted. There are two main effects visible, reduced amplitude and phase shift due to dispersion. The phases do not match, and mismatch increases with depth because of velocity dispersion in the attenuating media. For moderate attenuation values (Q=100), as shown in Figure 7b, the attenuation effects at different depths for a single and series of SLS mechanisms ($L = 1$, $L = 3$, and $L = 5$) are still significant compared to the black curves that represent the acoustic case (no attenuation). As the wave begins to propagate, the amplitudes for the acoustic and viscoacoustic cases are very similar, but when the propagation time increases and the wave reach greater depth, its amplitude is strongly attenuated especially for the case Q=20 (Figure 8a). Also, when the wave reaches grater depth, the single SLS mechanism is not so accurate because of a mismatch with the three relaxation mechanisms results(Figure 8b).

In the second example, we consider wave propagation within the acoustic Marmousi model. A portion of the velocity model, 6km wide and 3 km in depth, is illustrated in Figure 9a. A shot is positioned at a $500m$ distance and a depth of $12m$. From this point, a wave with a time dependence given by a zero-phase Ricker wavelet with a center frequency of $25Hz$ propagates into the model. We position an array of receivers at the same depth, $4m$ apart. The Q model includes constant quality factors with different values, while the background model has $Q = 100$ (Figure 9b). The first-order pressure-velocity viscoacoustic wave equation using PML absorbing boundary condition is used to compute the synthetic seismograms. The FD staggered-grid contains 4th-order accuracy in space and 2nd-order accuracy in time. In Figure 10 the FD synthetic data of acoustic and viscoacoustic with a series of SLS mechanisms ($L = 1$, $L = 3$, and $L = 3$) are displayed. The shots include first arrivals, multiples, reflections, refractions, and diffraction. The viscoacoustic simulation exhibits reduced amplitude (particularly multiples) and shifted phase due to velocity dispersion. There are two main effects visible, reduced amplitude and phase shift due to velocity dispersion. Trace number 600 for acoustic and viscoacoustic data ($L = 1$, $L = 3$, and $L = 5$) is illustrated in Figure 11. We can see that the viscoacoustic data are very

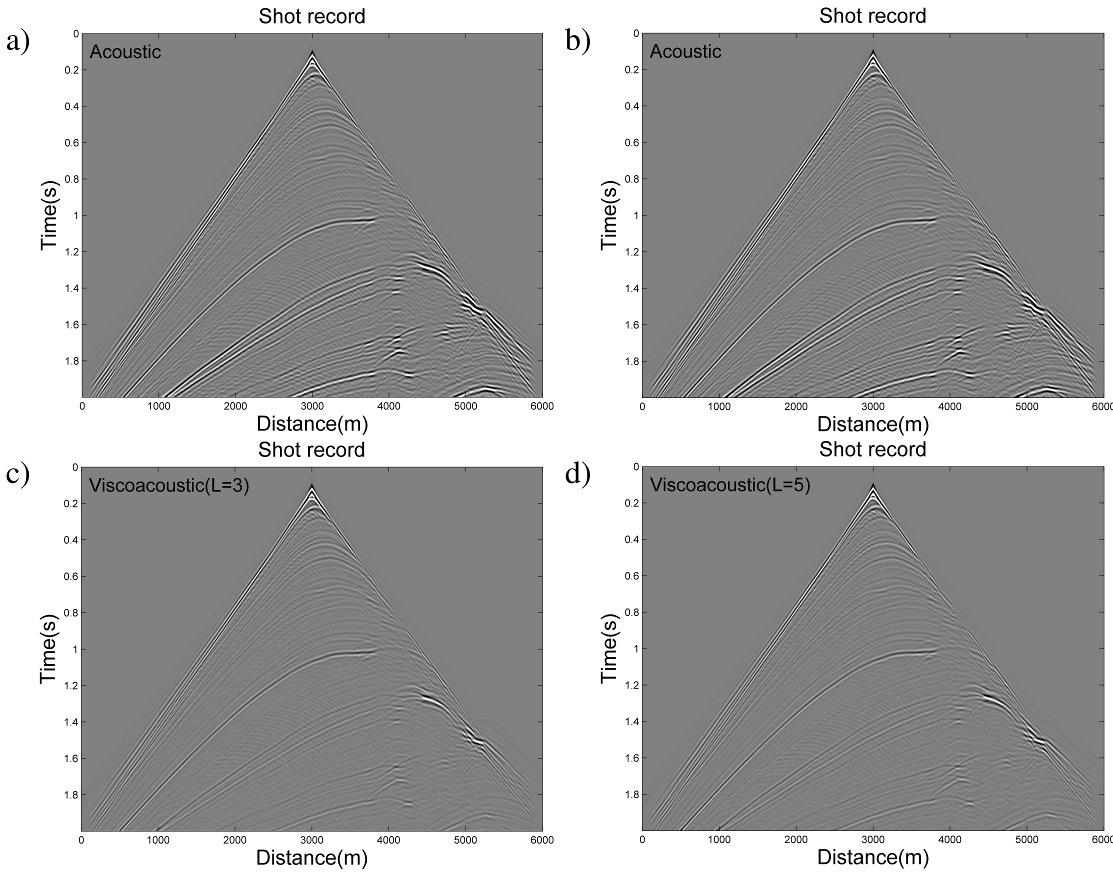

FIG. 10. Shot record from acoustic simulation (a), viscoacoustic ($L = 1$) simulation (b), viscoacoustic ($L = 3$) simulation, and viscoacoustic ($L = 5$) simulation using PML absorbing boundary condition.

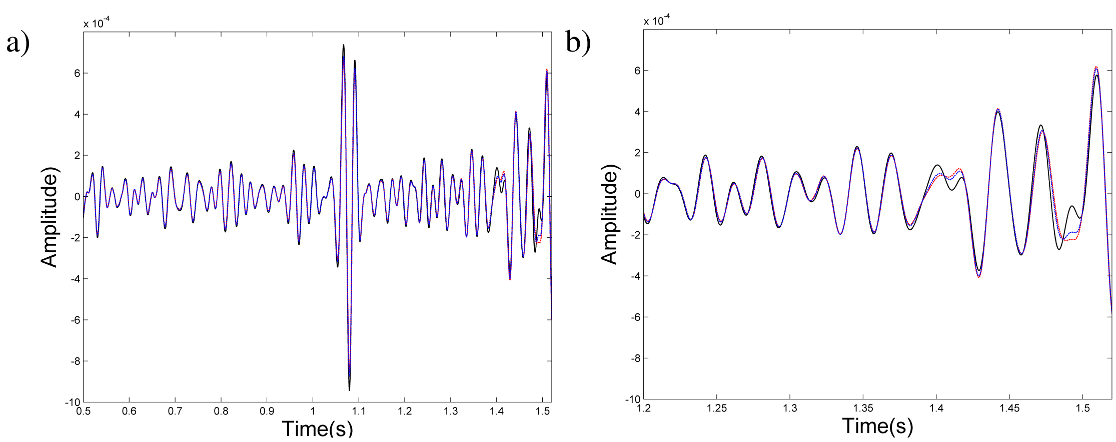

FIG. 11. Depth traces of FD showing the comparison trace number 150 of acoustic (black line), viscoacoustic ($L = 1$(dashed red line)) , and viscoacoustic ($L = 3$(dashed blue line)).

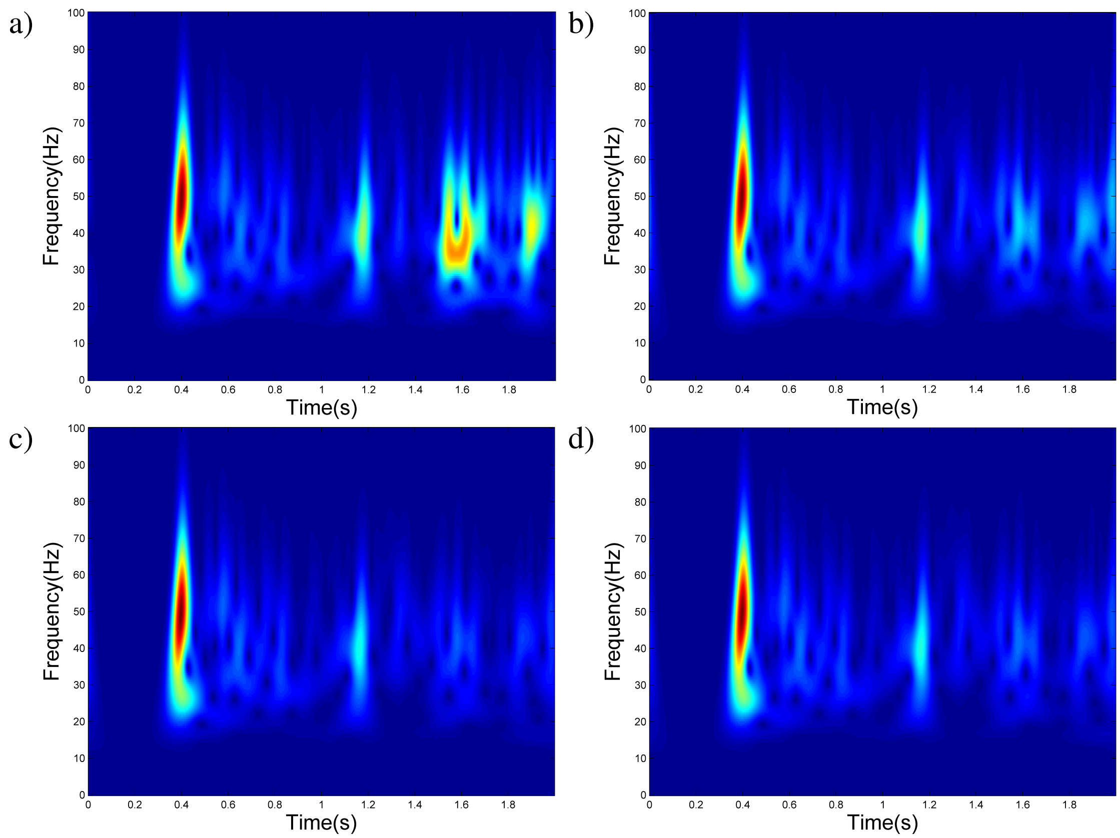

FIG. 12. The S spectrum of the shot record from acoustic simulation (a), viscoacoustic ($L = 1$) simulation (b), viscoacoustic ($L = 3$) simulation, and viscoacoustic ($L = 5$) simulation.

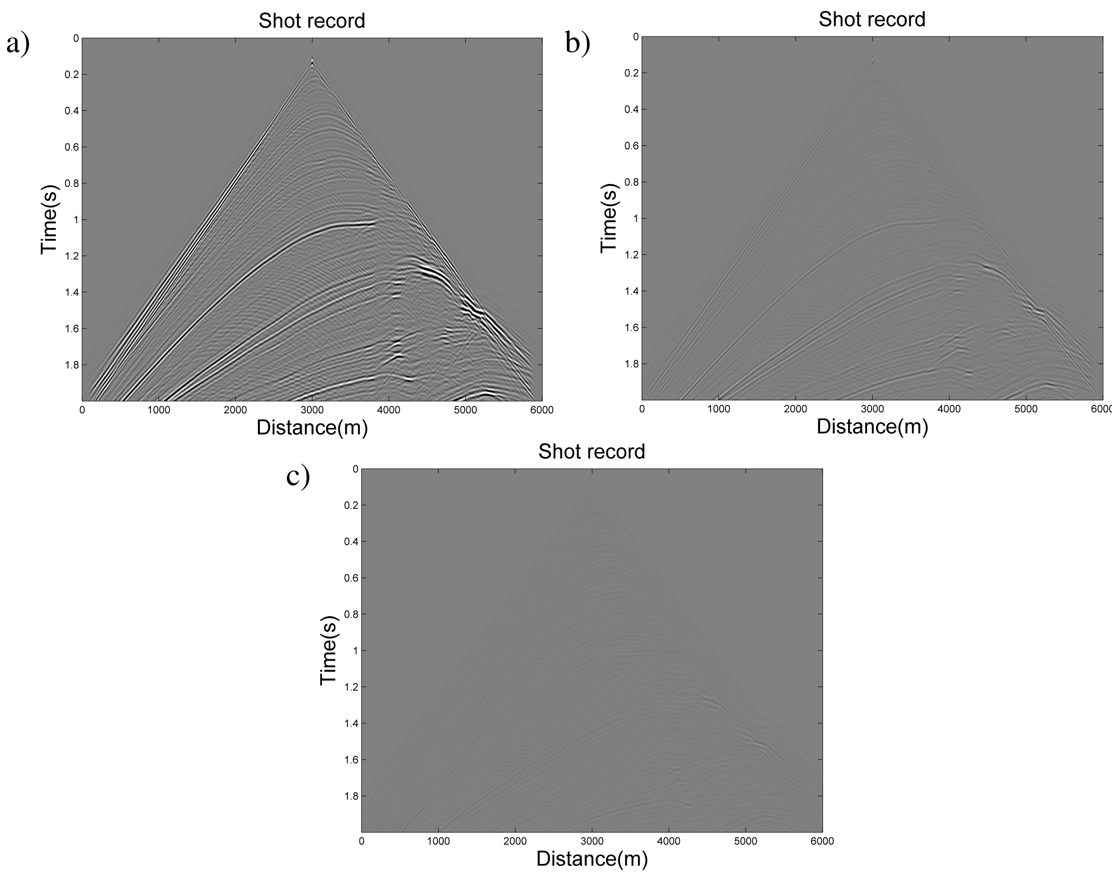

FIG. 13. Difference between acoustic and viscoacoustic data ($L = 3$) (a), viscoacoustic ($L = 3$) and viscoacoustic ($L = 1$) data, and viscoacoustic ($L = 3$) and viscoacoustic ($L = 5$). The viscoacoustic($L = 3$) and viscoacoustic ($L = 5$) are very close together.

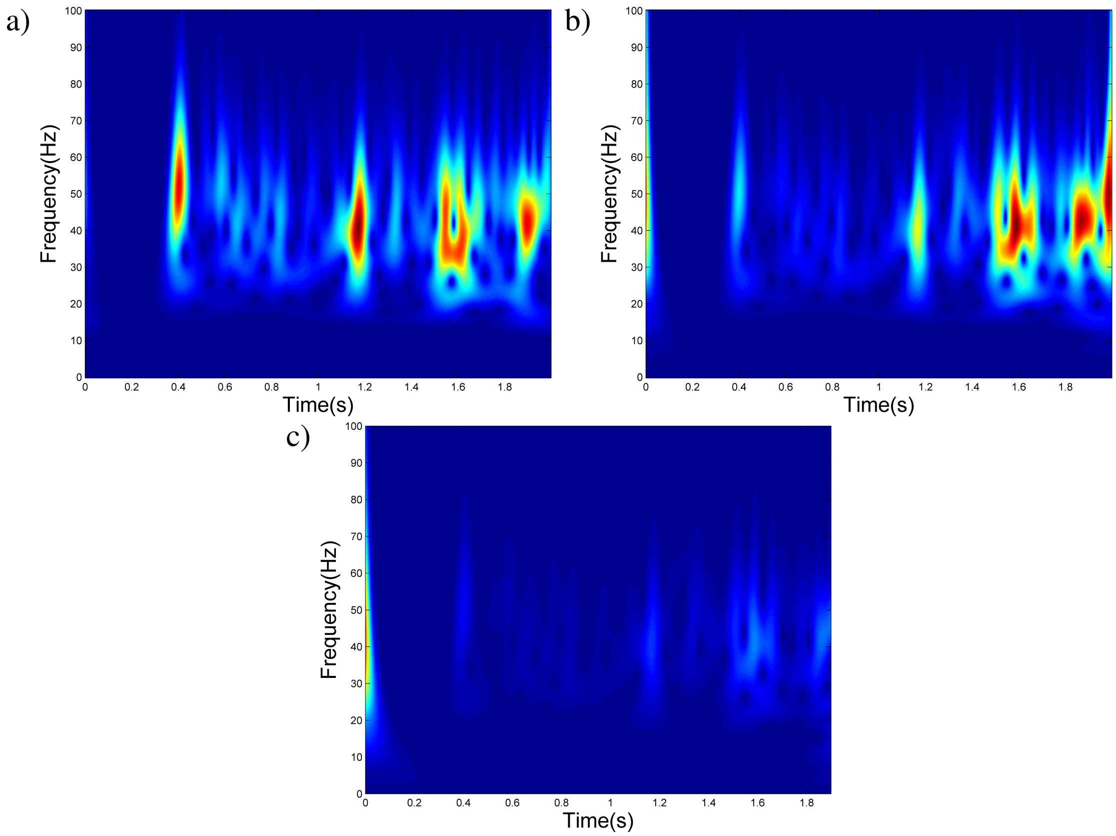

FIG. 14. The S spectrum of difference between acoustic and viscoacoustic data ($L = 3$) (a), viscoacoustic ($L = 3$) and viscoacoustic ($L = 1$) data, and viscoacoustic ($L = 3$) and viscoacoustic ($L = 5$). The viscoacoustic($L = 3$) and viscoacoustic ($L = 5$) are very close together.

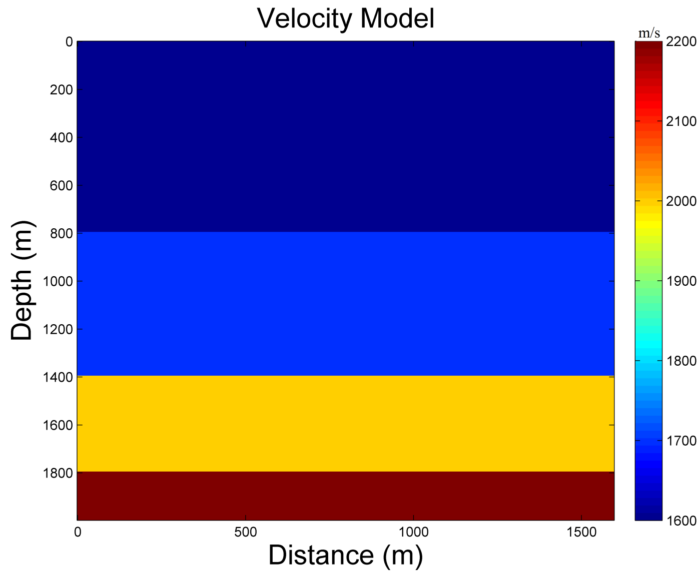

FIG. 15. The layered velocity model

similar together. However, the single SLS mechanism has some error compared with the three relaxation mechanisms in the gather depth with the strong attenuation. We know that in the attenuation media the reflection wave energy decay with the increase of the depth, so the frequency bandwidth become narrow, the high frequency more decay and the dominant frequency move to the low frequency(Figure 12). The difference waveforms between the acoustic and viscoacoustic data are shown in Figure 13. This figure include the difference waveforms between the acoustic and viscoacoustic data ($L = 3$) (Figure 13a), the viscoacoustic data($L3$) with viscoacoustic data($L = 1$) (Figure 13b), and the viscoacoustic data($L = 3$) with viscoacoustic data($L = 5$) (Figure 13c)results. For strong attenuation values, as the wave begins to propagate, the viscoacoustic ($L = 3$) and viscoacoustic ($L = 1$) data are very similar. When the wave reaches grater depth, the single SLS mechanism is not so accurate because of mismatch with the three relaxation mechanisms results(Figure 13b. In Figure 13c, two viscoacoustic data with $L = 3$ and $L = 5$ are close together, and there is no significant difference between them. The S spectrum of Figure 13 are shown in Figure 14.

REVERSE TIME MIGRATION

In this section, we consider the accuracy of nearly constant-Q wave propagation by series of standard linear solid (SLS) for RTM images with attenuation for a layered model using a time-space domain FD method. We use as the source a zero-phase Ricker wavelet with a center frequency of $25Hz$. The synthetic data are migrated by using the acoustic RTM and viscoacoustic RTM with a different number of mechanisms ($L = 1$, $L = 3$, and $L = 5$). Perfectly matched layer (PML) absorbing boundary conditions are used to attenuate the reflections from an artificial boundary. In Figure 15 a layered model is displayed. The model grid dimensions are 501×401, the grid size is 4 m ×4 m, and the quality factors for the background are $Q = 100$ and $Q = 20$ respectively. The sampling interval is $0.4ms$, and the recording length is $2s$.

For weak attenuation,i.e., constant $Q = 100$, the RTM images are shown in Figure 16,

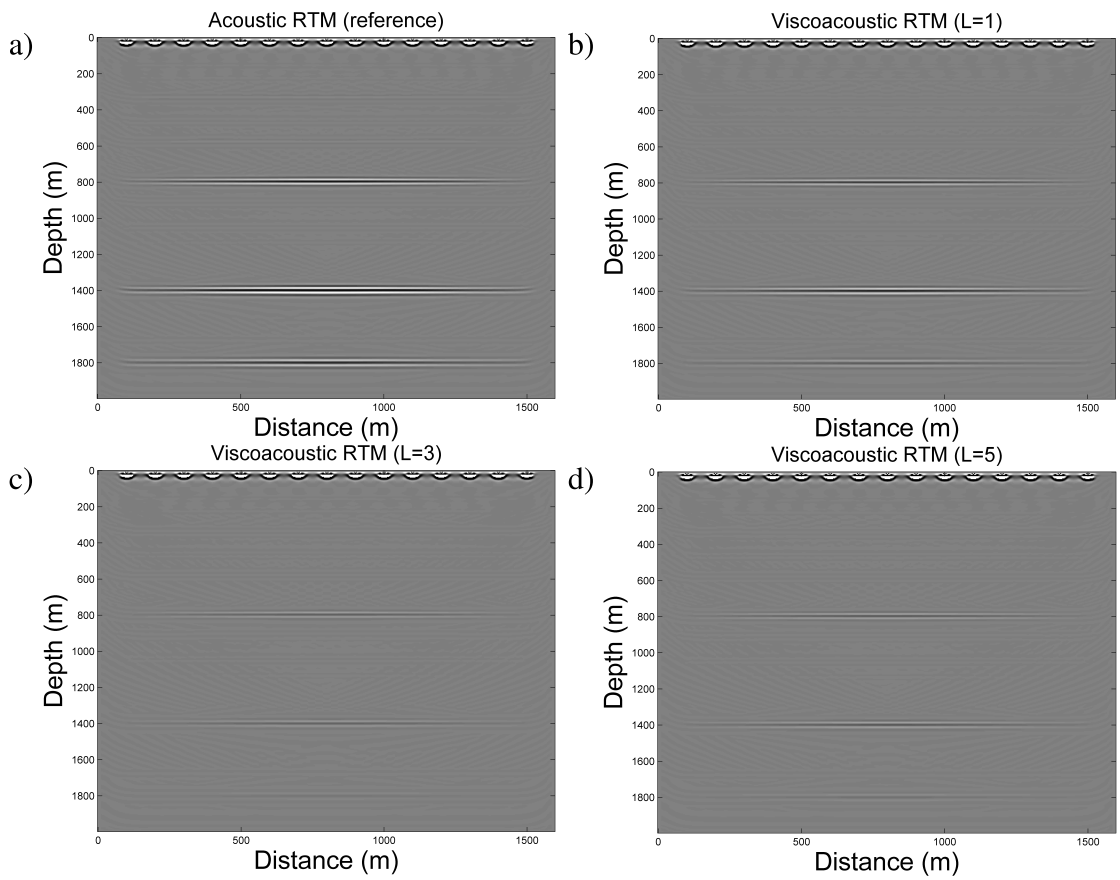

FIG. 16. The RTM images of the layered model with background attenuation ($Q = 100$) (a) acoustic RTM (reference), (b) viscoacoustic RTM ($L = 1$), (c) viscoacoustic RTM ($L = 3$) and (b)viscoacoustic RTM ($L = 5$).

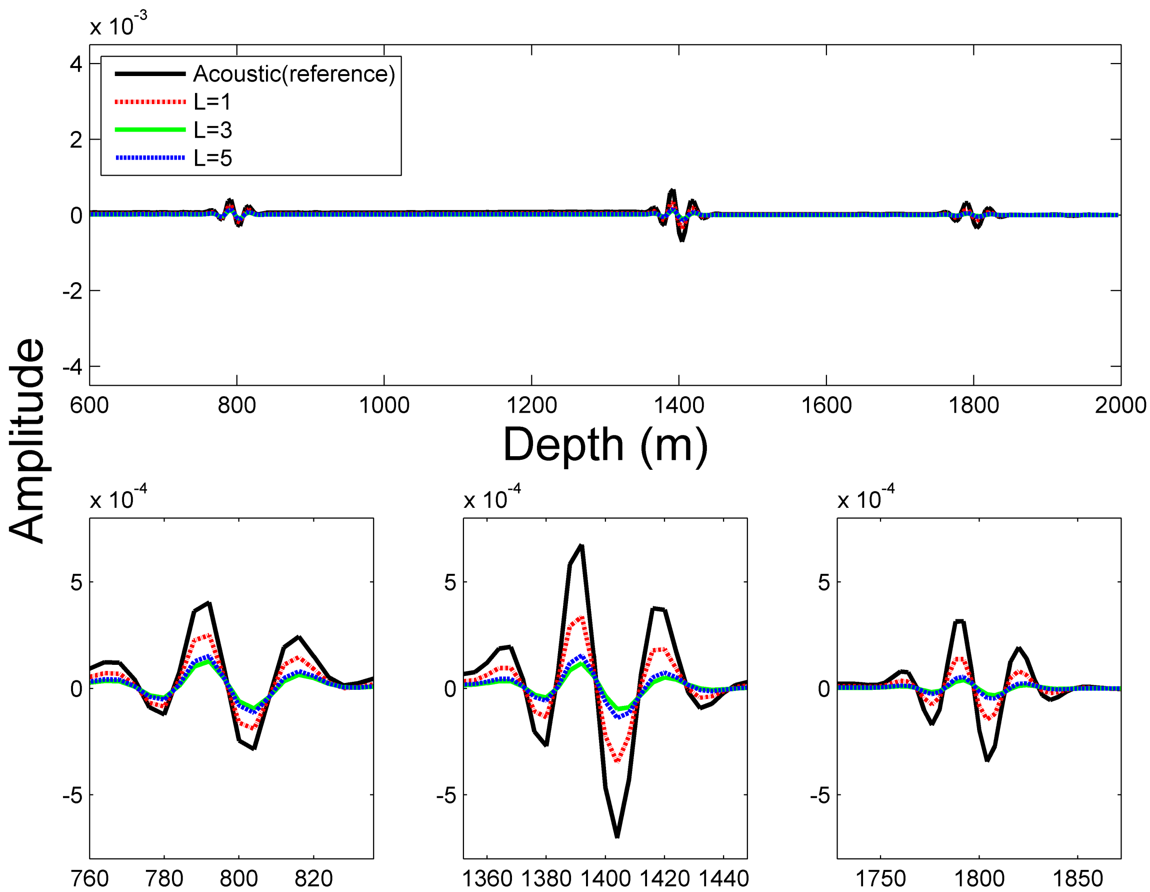

FIG. 17. Depth slices from Figure 13 showing the effect of attenuation and comparison of acoustic (Black solid line), viscoacoustic $L = 1$ (dashed red line), viscoacoustic $L = 3$ (green solid line), and viscoacoustic $L = 5$ (dashed blue line).

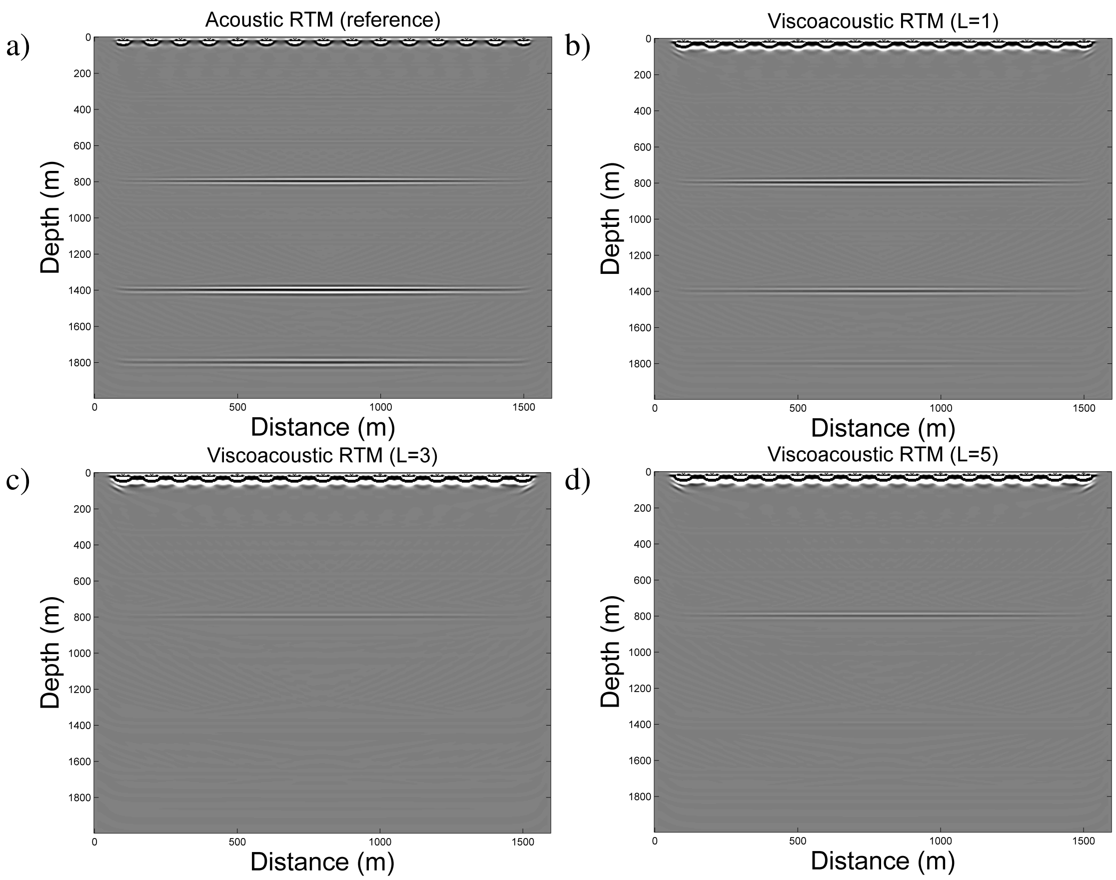

FIG. 18. The RTM images of the layered model with background attenuation ($Q = 20$) (a) acoustic RTM (reference), (b) viscoacoustic RTM ($L = 1$), (c) viscoacoustic RTM ($L = 3$) and (b)viscoacoustic RTM ($L = 5$).

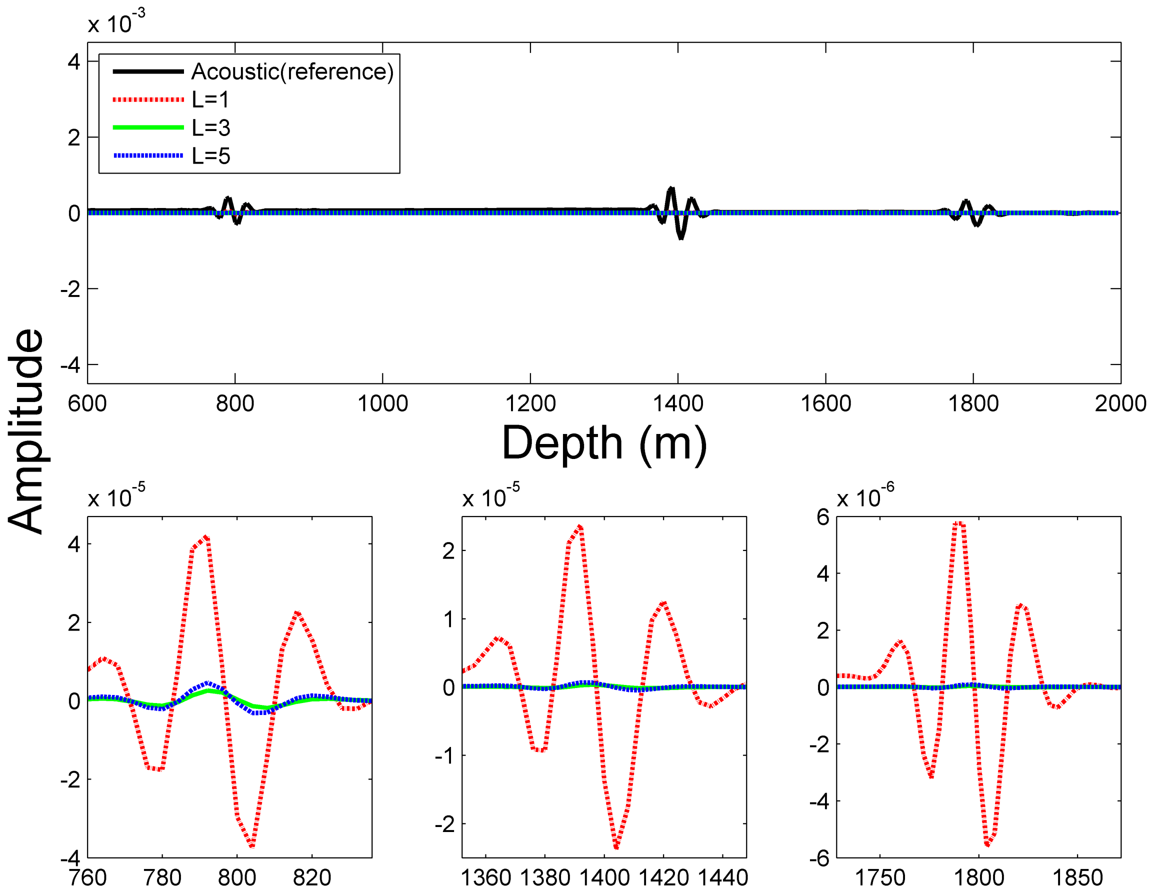

FIG. 19. Depth slices from Figure 15 showing the effect of attenuation and comparison of acoustic (Black solid line), viscoacoustic $L = 1$ (dashed red line), viscoacoustic $L = 3$ (green solid line), and viscoacoustic $L = 5$ (dashed blue line).

which includes the acoustic RTM without attenuation (reference) (Figure 16a), the viscoacoustic RTM with a different number of mechanisms (Figure 16b, c, and d) results. The attenuation affects the amplitudes and the phases of the propagating waves, effects which are not taken into account in the acoustic RTM image. In Figure 17 we compare the depth traces of acoustic and viscoacoustic data with a different number of SLS mechanisms. The acoustic and viscoacoustic RTM images have similar artifacts and amplitudes in the shallow layers. At the deep layers, we can see that the single, three, and five SLS mechanisms yield comparable results with the acoustic case.
For the strong attenuation value, i.e., constant $Q = 20$, the RTM images of the single, three, and five SLS mechanisms are shown in Figure 18 and compare with the acoustic case results. The viscoacoustic RTM images have very weak amplitudes in the deeper layers with strong attenuation (Figures 17b, c, and d). In Figure 19 we show a comparison of amplitudes between acoustic and viscoacoustic data. The three and five SLS mechanisms results agree very well together, while the single SLS mechanism is not so accurate than them. However in the deeper layer the error of single SLS mechanism increase, the results are still useful for practical application.

CONCLUSIONS

Time-domain approximate constant-Q wave propagation involving a series of standard linear solid (SLS) mechanisms is investigated. We found that the numerical results and analytical solutions using single and a series of standard linear solid (SLS) mechanisms in the weak attenuation medium agree very well. In strong attenuation when the wave reaches greater depth, the error of numerical solutions using single SLS mechanism increase and the viscoacoustic RTM images using a single SLS mechanisms are not so accurate. Although modeling of a single SLS relaxation mechanism is still useful for practical application and faster than three and five SLS mechanisms, the three SLS relaxation mechanisms are quite accurate for both weak and strong attenuation.

ACKNOWLEDGMENTS

The authors thank the sponsors of CREWES for continued support. This work was funded by Mitacs, CREWES industrial sponsors and NSERC (Natural Science and Engineering Research Council of Canada) through the grant CRDPJ 461179-13.

REFERENCES

Blanch, J. O., Robertsson, J. O., and Symes, W. W., 1995, Modeling of a constant q: Methodology and algorithm for an efficient and opti- mally inexpensive viscoelastic technique: Geophysics, **60**, 176–184.

Bourbie, T., Coussy, O., and Zinzner, B., 1987, Acoustic of porous media: Gulf publishing company.

Carcione, J. M., Kosloff, D., and Kosloff, R., 1988, Viscoacoustic wave propagation simulation in the earth: Geophysics, **53**, 769–777.

Casula, G., and Carcione, J. M., 1992, Generalized mechanical model analogies of linear viscoelastic behaviour: Bollettino di Geofisica Teorica ed Applicata, **34**, 235–256.

Christense, R. M., 1982, Theory of viscoelasticity: An introduction: Academic Pres.

Emmerich, H., and Korn, M., 1987, Incorporation of attenuation into time-domain computations of seismic wavefields: Geophysics, **52**, 1252–1264.

Fathalian, A., and Innanen, K., 2016, An unsplit-f i eld pml formulation for the 2d viscoacoustic wave equation in the time domain: modeling and imaging: crewews reports 2016.

Kjartansson, A., 1979, Constant-q wave propagation and attenuation: Journal of Geophysical Research, **84**, 4737–4748.

Liu, H. P., Anderson, D. L., and Kanamori, H., 1976, Velocity dispersion due to anelasticity: Implication for seismology and mantle composition: Geophysical Journal of the Royal Astronomical Society, **47**, 41–58.

McDonal, F. J., Angona, F. A., Mills, R. L., Sengbush, R. L., Nostrand, R. G. V., and White, J. E., 1958, Attenuation of shear and compressional waves in pierre shale: Geophysics, **23**, 421–439.

Robertsson, J. O. A., Blanch, J. O., and Symes, W. W., 1994, Viscoelastic finite-difference modeling: Geophysics: Geophysics, **59**, 1444–1456.

Savage, B., Komatitsch, D., and Tromp, J., 2010, Bulletin of the seismological society of america: Inverse Problems, **100**.